

Electronic Structure of Stripes in Two-Dimensional Hubbard Model

Masanori ICHIOKA* and Kazushige MACHIDA**

Department of Physics, Okayama University, Okayama 700-8530

(Received June 7, 1999)

Focusing on $\text{La}_{2-x}\text{Sr}_x\text{CuO}_4$, we study the stripe structure by the self-consistent mean-field theory of the Hubbard model. By introducing the realistic Fermi surface topology, the SDW-gapped insulator is changed to metallic. The solitonic features of the stripe structure and the contribution of the mid-gap states are presented. We consider the band dispersion, the local density of states, the spectral weight, and the optical conductivity, associated with the solitonic structure. These results may provide important information for the experimental research of the stripe structure, such as the angle-resolved photoemission experiments. The “Fermi surface” shape is changed depending on the ratio of the incommensurability δ and the hole density n_h . In real space, only the stripe region is metallic when δ/n_h is large.

KEYWORDS: Stripe structure, high T_c cuprates, Spectral weight, Hubbard model

§1. Introduction

The concept of the stripe structure is quite versatile and powerful in understanding various spatially modulated orderings ranging from insulator to metal, such as spin or charge density waves (SDW or CDW) or spin Peierls systems. A canonical example of such a stripe description is the incommensurate SDW in metallic Cr dilutely doped with Mn or V atoms. Various aspects of the SDW under doping are coherently describable in terms of the stripe.^{1,2)} Another canonical example for such description is the spin Peierls systems such as in CuGeO_3 or other organic materials under a magnetic field which effectively acts as changing the electron filling.^{3,4,5)} Thus, it is believed that the stripe concept is a useful paradigm for low dimensional electron systems with nearly half-fillings.

Anomalous electronic properties in under-doped high T_c cuprates attract much attention because understanding of the unusual ground state may lead us to a clue to a high T_c mechanism. One of the key features is the magnetic incommensurate (IC) structure, i.e., the stripe structure. Recently, the static magnetic IC structure is observed by the elastic neutron scattering on $\text{La}_{2-x}\text{Sr}_x\text{CuO}_4$ (LSCO).^{6,7,8,9)} It suggests the static stripe structure. The static IC structure is also reported on $\text{La}_{1.6-x}\text{Nd}_{0.4}\text{Sr}_x\text{CuO}_4$ [ref. 10] and $\text{La}_{2-x}\text{Sr}_x\text{NiO}_{4+y}$ [refs. 11 and 12].⁹⁾ In $\text{YBa}_2\text{Cu}_3\text{O}_{7-\delta}$, the IC fluctuations are reported by the inelastic neutron experiments.^{13,14)}

Almost a decade ago, one of the authors^{15,16)} predicts some of the features of the above static IC spin modulation in lightly doped cuprate systems, stressing the charged stripe or the solitonic structure as a convenient and universal “vehicle” to accommodate excess carriers in an otherwise commensurate antiferromagnetic (AF) state within a mean-field treatment for a simple two-

dimensional Hubbard model. Some features of them were independently found by others at that time^{17,18,19)} and later.^{20,21)} And they are now confirmed by a more sophisticated method, such as DMRG.²²⁾ But, since the above solitonic structure is an insulator in nature while high T_c cuprates are metallic, it was claimed that the other scenario such as frustrating charge segregation is needed.²³⁾ However, we can consider the metallic structure in the same framework of the selfconsistent mean-field theory, if the realistic Fermi surface topology is taken into account by introducing a next nearest neighbor site hopping. It is still important to study the detailed structure of the stripe state in this framework. The stripe state in the d - p model (i.e., including O-site contribution) was studied within the mean-field theory in ref. 24.

The purpose of this paper is to analyze the stripe structure based on the mean field method of the Hubbard model. Needless to say, the mean field theory which satisfies variational principle for the energy minimum can be justifiable when a long-range order exists, such as in the present case. Thermal or quantum fluctuations can be treated perturbatively from this solution, if it is needed. We consider the doping dependence and the effect of the realistic Fermi surface topology. Our numerical method is described in §2. The profile of the stripe structure and its band structure are studied in §3. We also discuss the doping dependence of the incommensurability. In §4, we study the density of states (DOS) and the local density of states (LDOS). The latter will be observed by scanning tunneling microscopy (STM) experiments. In §5, we discuss the spectral weight, i.e., \mathbf{k} -resolved DOS. Our results are compared with the data of the angle-resolved photoemission (ARPES) experiments,^{25,26,27,28)} which is a powerful method to study Fermi surface topology and pseudo-gap structure.²⁹⁾ In §6, we calculate the optical conductivity, which detects excitations of the stripe structure, and compare with the data.^{30,31)} Our theoretical study shows that these experimental methods can give us a lot of useful information of the stripe structure,

* E-mail: oka@mp.okayama-u.ac.jp

** E-mail: machida@mp.okayama-u.ac.jp

such as the mid gap state or the \mathbf{k} -dependent SDW gap. The last section is devoted to summary and discussions. Throughout this paper, we set $\hbar = k_B = 1$ and the lattice constant $c = 1$. Some of our results were briefly reported in ref. 32.

§2. Selfconsistent Mean-Field Theory

We start out with the standard Hubbard model on a two-dimensional square lattice and introduce the mean field

$$\langle n_{i,\sigma} \rangle = \frac{1}{2}(n_i + \sigma M_i) \quad (2.1)$$

at i -site, where n_i (M_i) is the charge (spin) density and $i = (i_x, i_y)$. Thus, the one-body Hamiltonian is given by

$$\begin{aligned} \mathcal{H} = & - \sum_{i,j,\sigma} t_{i,j} a_{i,\sigma}^\dagger a_{j,\sigma} \\ & + U \sum_{i,\sigma} \langle n_{i,-\sigma} \rangle n_{i,\sigma} - U \sum_i \langle n_{i,\downarrow} \rangle \langle n_{i,\uparrow} \rangle. \end{aligned} \quad (2.2)$$

where $n_{i,\sigma} = a_{i,\sigma}^\dagger a_{i,\sigma}$ ($\sigma = 1$ for \uparrow , -1 for \downarrow) and $a_{i,\sigma}^\dagger$ ($a_{i,\sigma}$) is a creation (annihilation) operator. For the nearest neighbor (NN) pairs (i, j) , $t_{i,j} = t$. For the next NN pairs situated on a diagonal position in a square lattice, $t_{i,j} = t'$. For the third neighbor pairs, which are situated along the NN bond direction, $t_{i,j} = t''$. For the stripe structure with the N site periodicity,

$$\langle n_{i,\sigma} \rangle = \sum_{0 \leq l < N} e^{il\mathbf{Q} \cdot \mathbf{r}_i} \langle n_{l\mathbf{Q},\sigma} \rangle, \quad (2.3)$$

where \mathbf{r}_i is the position of i -site. The modulation vector is given by $\mathbf{Q} = \mathbf{Q}_D = 2\pi(\frac{1}{2} - \delta, \frac{1}{2} - \delta)$ for diagonal incommensurate (DIC) state, $\mathbf{Q} = \mathbf{Q}_V = 2\pi(\frac{1}{2}, \frac{1}{2} - \delta)$ for vertical incommensurate (VIC) state, and $\mathbf{Q} = \mathbf{Q}_C = 2\pi(\frac{1}{2}, \frac{1}{2})$ for commensurate antiferromagnetic (C-AF) state. We set the incommensurability $\delta = M/N$ (rational fraction) with even integer N . We consider eq. (2.2) in the reciprocal space. There, \mathbf{k} is coupled to $\mathbf{k} + l\mathbf{Q}$ in the term $U \sum_{\mathbf{k}, l, \sigma} \langle n_{l\mathbf{Q},-\sigma} \rangle a_{\mathbf{k}+l\mathbf{Q},\sigma}^\dagger a_{\mathbf{k},\sigma}$, where $a_{\mathbf{k},\sigma}$ is the Fourier component of $a_{i,\sigma}$. We write $\mathbf{k} = \mathbf{k}_0 + m\mathbf{Q}$ ($m = 0, 1, \dots, N-1$), where \mathbf{k}_0 is within the reduced Brillouin zone of the size $(2\pi)^2/N$. Then, eq. (2.2) is reduced to

$$\mathcal{H} = \mathcal{H}_1 + \mathcal{H}_2 \quad (2.4)$$

$$\begin{aligned} \mathcal{H}_1 = & \sum_{\mathbf{k}_0, \sigma, m} \left\{ \epsilon(\mathbf{k}_0 + m\mathbf{Q}) a_{\mathbf{k}_0+m\mathbf{Q},\sigma}^\dagger a_{\mathbf{k}_0+m\mathbf{Q},\sigma} \right. \\ & \left. + U \sum_{0 < l < N} \langle n_{l\mathbf{Q},-\sigma} \rangle a_{\mathbf{k}_0+(m+l)\mathbf{Q},\sigma}^\dagger a_{\mathbf{k}_0+m\mathbf{Q},\sigma} \right\} \\ = & \sum_{\mathbf{k}_0, \sigma, \alpha} E_{\mathbf{k}_0, \sigma, \alpha} \gamma_{\mathbf{k}_0, \sigma, \alpha}^\dagger \gamma_{\mathbf{k}_0, \sigma, \alpha}, \end{aligned} \quad (2.5)$$

$$\begin{aligned} \mathcal{H}_2 = & U \sum_{\mathbf{k}_0, \sigma, m} \bar{n}_{-\sigma} a_{\mathbf{k}_0+m\mathbf{Q},\sigma}^\dagger a_{\mathbf{k}_0+m\mathbf{Q},\sigma} \\ & - UN_k \sum_{0 \leq l < N} \langle n_{l\mathbf{Q},\uparrow} \rangle \langle n_{l\mathbf{Q},\downarrow} \rangle, \end{aligned} \quad (2.6)$$

where $\bar{n}_\sigma = \langle n_{l=0,\sigma} \rangle$ is the average number of σ -spin electron per site, $N_k = \sum_i 1 = \sum_{\mathbf{k}_0, m} 1$, and $\epsilon(\mathbf{k}) = \epsilon_0(\mathbf{k}) + \epsilon_1(\mathbf{k})$ with $\epsilon_0(\mathbf{k}) = -2t(\cos k_x + \cos k_y)$ and $\epsilon_1(\mathbf{k}) = -4t' \cos k_x \cos k_y - 2t''(\cos 2k_x + \cos 2k_y)$. In eq. (2.5), we diagonalize $N \times N$ matrix \mathcal{H}_1 by using the unitary transformation

$$a_{\mathbf{k}_0+m\mathbf{Q},\sigma} = \sum_{\alpha} u_{\mathbf{k}_0, \sigma, \alpha, m} \gamma_{\mathbf{k}_0, \sigma, \alpha}, \quad (2.7)$$

where $\alpha (= 1, 2, \dots, N)$ is the label of the eigen-energy $E_{\mathbf{k}_0, \sigma, \alpha}$ and the wave function $u_{\mathbf{k}_0, \sigma, \alpha, m}$.

The self-consistent condition is given by

$$\begin{aligned} \langle n_{l\mathbf{Q},\sigma} \rangle = & N_k^{-1} \sum_{\mathbf{k}_0, m} \langle a_{\mathbf{k}_0+m\mathbf{Q},\sigma}^\dagger a_{\mathbf{k}_0+(m+l)\mathbf{Q},\sigma} \rangle \\ = & N_k^{-1} \sum_{\mathbf{k}_0, m, \alpha} u_{\mathbf{k}_0, \sigma, \alpha, m}^* u_{\mathbf{k}_0, \sigma, \alpha, m+l} f(E_{\mathbf{k}_0, \sigma, \alpha}). \end{aligned} \quad (2.8)$$

Here, we use $\langle \gamma_{\mathbf{k}_0, \sigma, \alpha}^\dagger \gamma_{\mathbf{k}_0, \sigma, \alpha'} \rangle = \delta_{\alpha, \alpha'} f(E_{\mathbf{k}_0, \sigma, \alpha})$ with the Fermi distribution function $f(E) = (e^{(E-\mu)/T} + 1)^{-1}$.

In our calculation, the eigen-energy and the wave functions are obtained by eq. (2.5) under the given $\langle n_{l\mathbf{Q},\sigma} \rangle$. The chemical potential μ is determined by the condition $\bar{n}_\uparrow = \bar{n}_\downarrow = \frac{1}{2}(1 - n_h)$ for $1 - n_h$ filling. Then, we calculate $\langle n_{l\mathbf{Q},\sigma} \rangle$ by eq. (2.8), and use it in the next step calculation of eq. (2.5). This iteration procedure is repeated until a sufficient self-consistent solution is obtained. Among the possible stripe structures (C-AF, DIC and VIC with various incommensurability δ), the stable structure is determined by the total energy ($\langle \mathcal{H} \rangle$) minimum at zero temperature. We mainly consider the case $t' = -\frac{1}{6}t$ and $t'' = 0$. This set of the parameters is proposed for LSCO to reproduce the Fermi surface obtained by the band calculation.^{33, 34, 35)}

§3. Spatial Profile and Band Structure

For $t' = 0$, since the Fermi surface is almost a square shape near half-filling ($n_h \sim 0$), the complete nesting occurs, and one dimensional (1D) picture may be applicable.¹⁵⁾ By introducing the effect of t' , the Fermi surface deviates from the square shape. At first, we consider the t' -effect on the C-AF state. The energy dispersion is split into the upper conduction band and the lower valence band, and it is given by

$$\begin{aligned} E_{\pm}(\mathbf{k}) = & \frac{1}{2}[\epsilon(\mathbf{k}) + \epsilon(\mathbf{k} + \mathbf{Q}_C) \\ & \pm \{(\epsilon(\mathbf{k}) - \epsilon(\mathbf{k} + \mathbf{Q}_C))^2 + 4|\Delta_{AF}|^2\}^{1/2}] \\ = & \epsilon_1(\mathbf{k}) \pm \{\epsilon_0(\mathbf{k})^2 + |\Delta_{AF}|^2\}^{1/2}, \end{aligned} \quad (3.1)$$

with the AF gap Δ_{AF} . The AF gap opens at $\mathbf{k}_Q = (k_x, \pm\pi - k_x)$ and $(k_x, \pm\pi + k_x)$ by the nesting of \mathbf{Q}_C . Then, the lower and upper edges of the AF gap are written as $E_{\pm}(\mathbf{k}_Q) = \epsilon_1(\mathbf{k}_Q) \pm \Delta_{AF}$. For $t' < 0$, $E_{\pm}(\mathbf{k}_Q)$ is small near $(1, 0)$ and $(0, 1)$ in reciprocal lattice units compared with near $(\frac{1}{2}, \frac{1}{2})$, while the gap $E_+(\mathbf{k}_Q) - E_-(\mathbf{k}_Q) = 2\Delta_{AF}$ does not depend on the \mathbf{k} -point. This dispersive AF gap structure is in fact observed by ARPES on some parent compounds of High

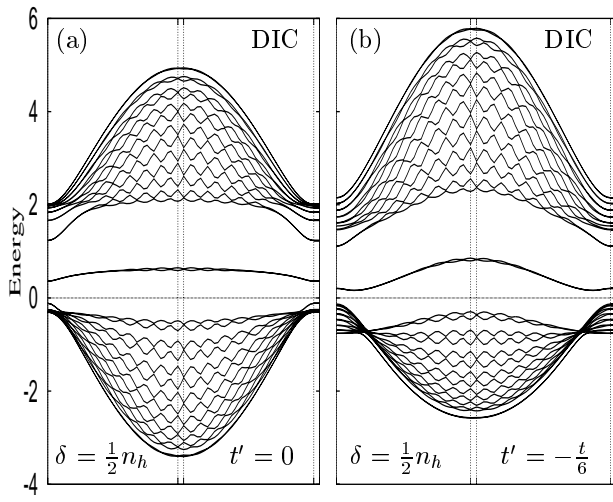


Fig. 1. Dispersion relations for DIC along the perimeter of the reduced Brillouin zone for $n_h = 1/16 = 0.0625$, $U = 3.6t$, $\delta/n_h = 1/2$. $t'/t = 0$ (a) and $-1/6$ (b). The Fermi energy E_F is at zero. Energy is scaled by t .

T_c superconductors such as a half-filled Mott insulator $\text{Ca}_2\text{CuO}_2\text{Cl}_2$.²⁵⁾

Next, we consider the t' -effect on the IC state for finite n_h . We also find the dispersive gap structure in the SDW gap. We show the energy dispersion within the reduced Brillouin zone in Fig. 1 for DIC and in Fig. 2 for VIC in the case $n_h = 1/16 = 0.0625$. There, a large SDW (or AF) gap opens between the conduction band and valence band, and there are some mid-gap bands in the large SDW gap. In the figure, unit vectors of the reduced Brillouin zone are given by $\mathbf{u}_1 = (0, 2\pi)$, $\mathbf{u}_2 = (2\pi/N, 2\pi/N)$ for DIC, and $\mathbf{u}_1 = (\pi, \pi - 2\pi M/N)$, $\mathbf{u}_2 = (0, 4\pi/N)$ for VIC. The horizontal axes in Figs. 1 and 2 are along the path $\frac{1}{2}(\mathbf{u}_1 + \mathbf{u}_2) - \frac{1}{2}\mathbf{u}_2 - \mathbf{o} - \frac{1}{2}\mathbf{u}_1 - \frac{1}{2}(\mathbf{u}_1 + \mathbf{u}_2)$.

In the stripe structure with N/M periodicity (i.e., M periods in N sites), the size of the Brillouin zone is reduced to $1/N$, and the energy dispersion is split to N bands as seen in Figs. 1 and 2. If it were half-filling, lower $N/2$ bands would be occupied by electrons. In the case of finite doping $n_h = M/(N/2)$, the induced holes enter M bands among $N/2$ bands. Then, an SDW gap opens above the fully occupied $N/2 - M$ bands, and $2M$ bands above the filled bands form a mid-gap state. Since the gapped state minimizes the total energy, the stripe structure with N/M periodicity is stable in an insulator state. Then, the incommensurability is exactly given by $\delta = M/N = \frac{1}{2}n_h$ in this insulator state. This relation between the incommensurability δ and the hole density n_h is confirmed by our energy estimate at $T = 0$ in the insulator state, even for finite t' . This is a generic statement which might be important to interpret the neutron diffraction experiments.^{6, 7, 8, 9, 10, 11, 12)}

For $t' = 0$, the lower and upper edges of the SDW gap are almost flat [Figs. 1(a) and 2(a)]. But, for finite t' , the gap edges become dispersive [Figs. 1(b) and 2(b)-(d)]. With increasing $|t'|$, both the valence band and the mid-gap state touch the Fermi energy E_F in the VIC case

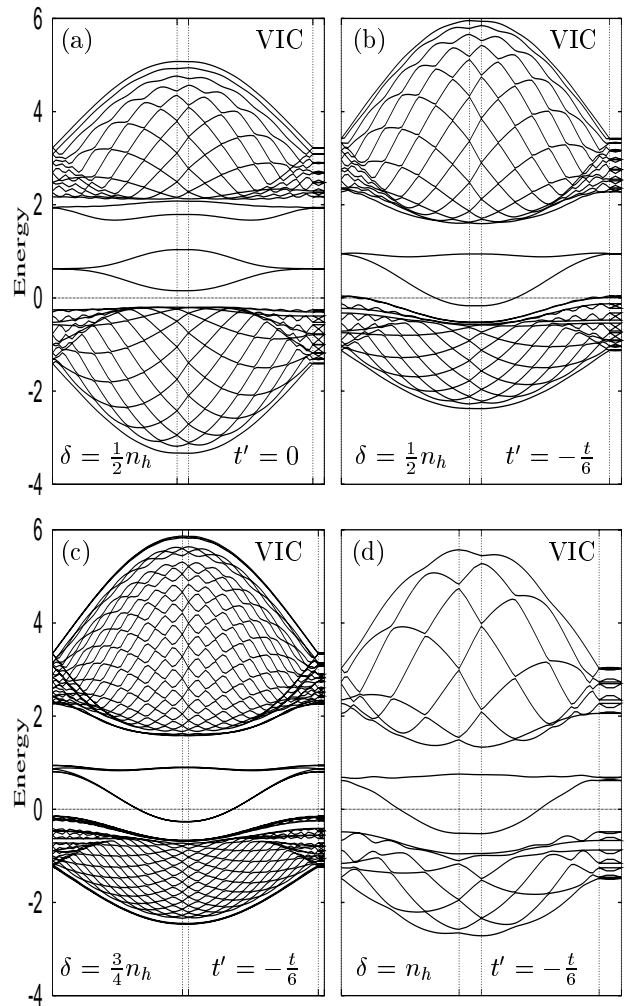


Fig. 2. Dispersion relations for VIC along the perimeter of the reduced Brillouin zone for $n_h = 1/16 = 0.0625$, $U = 3.6t$. (a) $t'/t = 0$ and $\delta/n_h = 1/2$. (b) $t'/t = -1/6$ and $\delta/n_h = 1/2$. (c) $t'/t = -1/6$ and $\delta/n_h = 3/4$. (d) $t'/t = -1/6$ and $\delta/n_h = 1$. The Fermi energy E_F is at zero. Energy is scaled by t .

with $\delta = \frac{1}{2}n_h$. And the stripe state becomes metallic [Fig. 2(b)]. We set $E_F = 0$ in the figures. For smaller U , it becomes easily metallic since the SDW gap is small.

The total energy of DIC is lower than that of VIC for higher U and smaller n_h .^{16, 18, 32)} For example, the DIC is stable for $n_h < n_c \sim 0.1$ in the case $U = 3.6t$ and $t' = -\frac{1}{6}t$. With raising (lowering) U , n_c increases (decreases). When $|t'|$ is larger, n_c decreases. The DIC state is difficult to become metallic since the dispersion of the mid-gap state is flat as shown in Fig. 1. While the metallic DIC state can be realized for larger n_h and smaller U , the VIC state is stable in these parameter regions. In the parameter region of the stable DIC, it is an insulator. Therefore, it is unlikely that the DIC is realized to be metallic upon doping. This is a generic statement within the present framework.

On the other hand, for the electron doping case ($n_h < 0$), the C-AF state has lower energy than those of VIC and DIC for small $|n_h|$ and lower U . And the VIC is stable for large $|n_h|$ and higher U . The DIC state does not appear for $n_h < 0$. The stable VIC's parameter region becomes narrower with increasing $|t'|$. The VIC

for $n_h < 0$ is an insulator, because the top of the mid-gap band is flat as seen in Fig. 2(b). E_F is located in the gap between the mid-gap band and the upper conduction band.

Once the metallic state is realized for $n_h > 0$, the relation $\delta = \frac{1}{2}n_h$, which is valid for the insulating case due to the energy gain by the SDW gap, is not obeyed. Figure 3 shows the n_h dependence of δ for VIC by our estimate of the total energy minimum. There, t'/t is changed from 0 to -0.2 , and $t'' = 0$. It is found that δ is fixed to be $\frac{1}{2}n_h$ in insulator state ($t'/t = 0, -0.05$). But, in metallic state of VIC, δ becomes larger than the $\frac{1}{2}n_h$ -line, and approach the n_h -line with increasing $|t'|$. The n_h -dependence is almost linear at small n_h , and slightly suppressed at large n_h . The n_h dependence of δ dose not depend on U in the metallic state for $3 \leq U/t \leq 4$. It only depends on t' , i.e., the shape of the Fermi surface. It may be related to the nesting of \mathbf{Q} vector. Figure 4 shows the Fermi surface of $\epsilon(\mathbf{k})$ for $n_h = 0.125$ and the \mathbf{Q}_V -shifted Fermi surface. The nesting seems to be better in the case $\delta \sim \frac{3}{4}n_h$ than in the case $\delta \sim \frac{1}{2}n_h$. It is the reason why δ is larger than $\frac{1}{2}n_h$. With increasing n_h further, the parameter δ/n_h for the best nesting is shifted to smaller. Then, the saturation of δ occurs at larger n_h as seen from Fig. 3. We also consider the case $t' = -0.12t$ and $t'' = 0.08t$. These parameters are proposed to reproduce the Fermi surface obtained by the ARPES experiments.^{27,28,36} The obtained δ is near the n_h -line, as shown by filled circles in Fig. 3. We note that the C-AF state has lower energy than VIC and DIC for small n_h in the case U is small and δ/n_h approaches 1. As a result, $\delta = \frac{1}{2}n_h$ for insulator DIC and VIC. And for metallic VIC, δ approaches $\delta = n_h$ with increasing $|t'|$ or $|t''|$. As for the DIC case, $\delta = \frac{1}{2}n_h$ in the insulator state. In the metallic DIC, which is difficult to be stable, δ is suppressed than $\frac{1}{2}n_h$ -line.

Some of our results are consistent with the experimental results. The elastic and inelastic neutron scattering experiments suggest that the insulator $\text{La}_{2-x}\text{Sr}_x\text{NiO}_{4+y}$ is DIC with $\delta \sim \frac{1}{2}n_h$.^{9,11,12} The metallic (or superconducting) LSCO for $x > 0.06$ and $\text{La}_{1.6-x}\text{Nd}_{0.4}\text{Sr}_x\text{CuO}_4$ are VIC.^{6,7,8,9,10} There, it is suggested that $\delta \sim n_h$ for small n_h . The saturation of δ occurs for large n_h , where the inter-stripe distance is close to the width of each stripe as shown later in Fig. 5(b). The upper limit of δ seems to be determined by the width of each stripe, beyond which δ saturates. The LSCO exhibits the transition from metallic to insulator at $x \sim 0.05$. With this transition, VIC with $\delta \sim x$ ($\sim n_h$) is changed to DIC with $\delta \sim \frac{1}{2}x$ [in the notation of ref. 6, $\mathbf{Q}_D = 2\pi(\frac{1}{2} - \frac{\epsilon}{2}, \frac{1}{2} - \frac{\epsilon}{2})$ with $\epsilon \sim n_h$]. Reference 6 reported that $\epsilon = 0.06 \pm 0.005$ at $x = 0.05$ in DIC. Also in our model, VIC is changed to DIC at critical n_h with decreasing n_h for appropriate U . The DIC is insulator with $\delta = \frac{1}{2}n_h$, and VIC can be metallic. Our model shows that δ becomes larger than $\frac{1}{2}n_h$ in the metallic VIC case. But, it fails to give the relation exactly $\delta = n_h$. To improve this point, we need to carefully adjust the parameters of the Fermi surface topology.³⁷ On this problem, the effect of the long range Coulomb interaction was also sug-

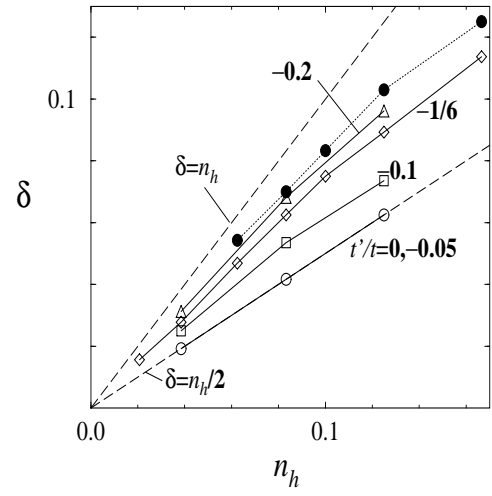


Fig. 3. The n_h dependence of the incommensurability δ to minimize the total energy for VIC. Open symbols with solid lines are for $t'/t = 0, -0.05$ (insulator), $-0.1, -1/6, -0.2$ (metal). Filled circles with a dotted line are for $t' = -0.12t$ and $t'' = 0.08t$. The lines are guide for the eye. In metallic case, δ is enhanced with increasing $|t'|$. We also show lines for $\delta = n_h$ and $\delta = n_h/2$ (dashed lines).

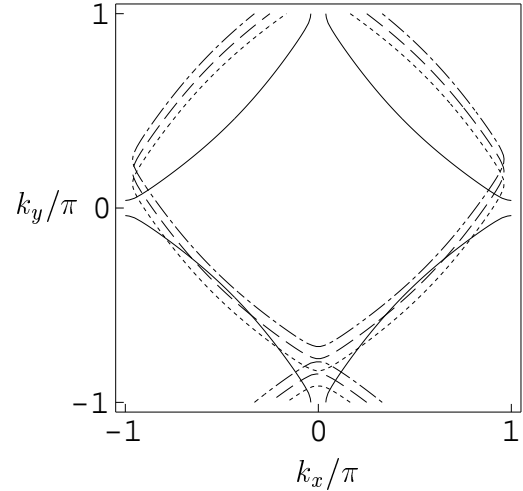


Fig. 4. Nesting features: the original Fermi surface of $\epsilon(\mathbf{k})$ [solid lines] and \mathbf{Q}_V -shifted ones for $\delta/n_h = 1/2$ [dotted lines], $3/4$ [dashed lines] and 1 [dash-dotted lines]. $n_h = 0.125$, $t'/t = -1/6$, $t'' = 0$. The $2\pi \times 2\pi$ Brillouin zone is presented. The nesting is seen to be better for $\delta/n_h \sim 3/4$ than $1/2$ or 1 .

gested.³⁸ There is a possibility that the VIC state with $\delta = n_h$ becomes more stable by adding the long range Coulomb interaction to the Fermi surface topology effect.

To see the effect of the δ shift on the gap structure at fixed n_h , we show the energy dispersion for $\delta = \frac{3}{4}n_h$ (c) [which gives the total energy minimum] and $\delta = n_h$ (d) in Fig. 2. They show qualitatively the same band structure as in the case $\delta = \frac{1}{2}n_h$ [Fig. 2(b)]. But, the position of E_F is changed depending on δ . With increasing δ at fixed n_h (i.e., effectively decreasing n_h compared with δ), E_F is shifted toward higher energy in the band structure. Both the valence band and the mid-gap state cross E_F for $\delta = \frac{1}{2}n_h$. For $\delta = \frac{3}{4}n_h$ and $\delta = n_h$, only the mid-gap

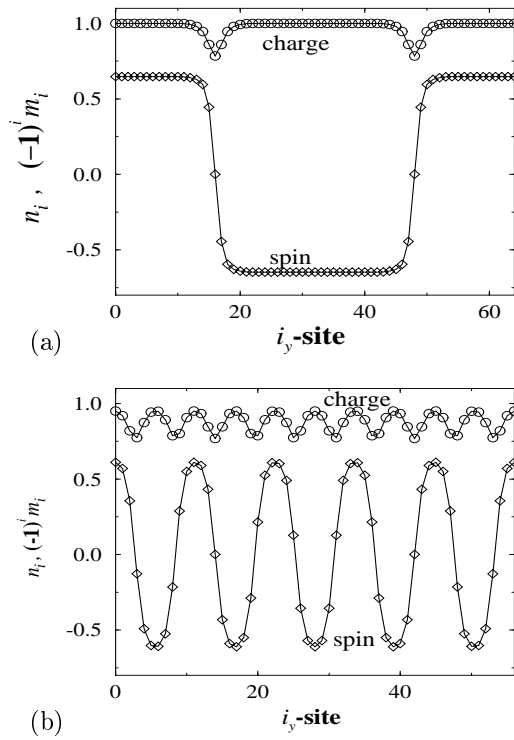


Fig. 5. The spatial profile of the charge density n_i and the magnetization $(-1)^{i_x+i_y}m_i$ along the y -direction in VIC. $U = 3.6t$, $t'/t = -1/6$. (a) $n_h = 1/48 = 0.021$, $\delta/n_h = 3/4$. (b) $n_h = 1/8 = 0.125$, $\delta/n_h = 5/7$.

state crosses E_F , and the valence band does not appear at E_F . In the following, we consider the optimized δ case shown in Fig. 3 ($\delta \sim \frac{3}{4}n_h$ for $t' = -\frac{1}{6}t$). But the result is not qualitatively changed for other δ . To know other δ cases, it is enough to shift E_F in the following results, keeping the overall gap structure unchanged.

Next, we discuss the spatial profile of the stripe structure. In Fig. 5, we show the spatial profiles of the charge density n_i and the magnetization $(-1)^{i_x+i_y}m_i$ along the y -direction. The excess carriers are located in the stripe region, and form CDW. The width of the charged stripe is about 3 sites in this case. The AF changes its phase by π when it crosses the stripe region. The envelope of m_i looks like sinusoidal wave for large n_h , but it looks like square wave for small n_h . To clearly see this profile change, we consider the Fourier components $n_{lQ} = n_{lQ,\uparrow} + n_{lQ,\downarrow}$ and $m_{lQ} = n_{lQ,\uparrow} - n_{lQ,\downarrow}$. In Fig. 6, we plot the n_h -dependence of m_{lQ}/m_Q ($l = 3, 5, 7$) and n_{lQ}/m_Q ($l = 2, 4, 6$). For large n_h , $m_{lQ}/m_Q \rightarrow 0$ ($l \geq 3$). It means that the fundamental component m_Q is dominant and that m_i varies as a simple sinusoidal wave. On the other hand, with decreasing n_h , $m_{lQ}/m_Q \rightarrow (-1)^{(l-1)/2}/l$ ($l \geq 3$: odd integer). It is the Fourier component of the square wave. The continuous change from the sinusoidal wave to the square wave with decreasing n_h is reminiscent of the Jacobi elliptic function $sn(x, k)$, which was the form in 1D CDW or SDW systems near the half-filling.¹⁵⁾

This n_h -dependence of the m_i -profile is expected to be observed by several experiments. We show the n_h -

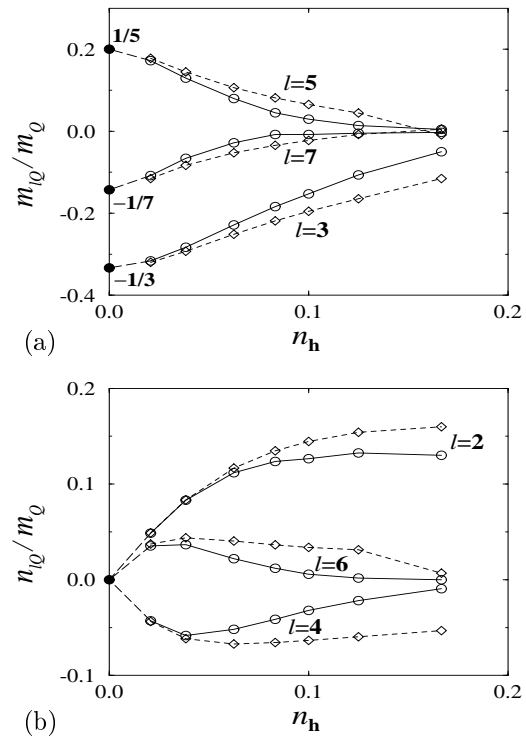


Fig. 6. The n_h -dependence of the higher harmonics of the Fourier components, m_{lQ} (a) and n_{lQ} (b) for VIC (\circ) and DIC (\diamond). We plot m_{lQ}/m_Q ($l = 3, 5, 7$) and n_{lQ}/m_Q ($l = 2, 4, 6$), respectively. Lines are guide for the eye, and \bullet shows the extrapolation for $n_h \rightarrow 0$. $U = 3.6t$, $t'/t = -1/6$. We use the optimized value of δ given in Fig. 3

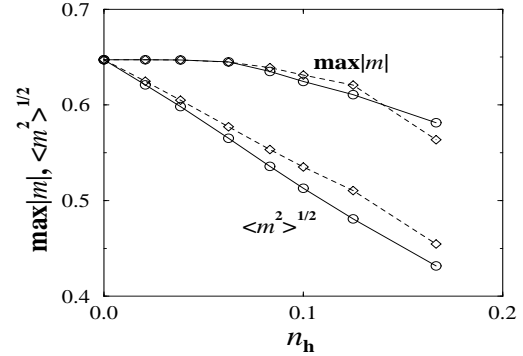


Fig. 7. The n_h -dependence of the maximum ($\max|m_i|$) and the variance ($\langle m_i^2 \rangle^{1/2}$) of the magnetization in VIC (\circ) and DIC (\diamond). $U = 3.6t$, $t'/t = -1/6$.

dependence of the maximum $\max|m_i|$, and the variance $\langle m_i^2 \rangle^{1/2}$. As shown in Fig. 7, $\max|m_i|$ sustains a constant for $0 < n_h < 0.06$, but $\langle m_i^2 \rangle^{1/2}$ decreases gradually with increasing n_h . That is, in the experiments which detect the maximum of the magnetic moment such as the neutron scattering, the magnetization does not depend on n_h for small n_h . But, in the experiments which detect the spatial average of the magnetic moment such as NMR, the magnetization gradually decreases with increasing n_h . This distinction is observed in Cr.^{1,2)} As seen in Fig. 8, the distribution function $P(m)$ of the magnetic moment (i.e., the resonance line shape of NMR

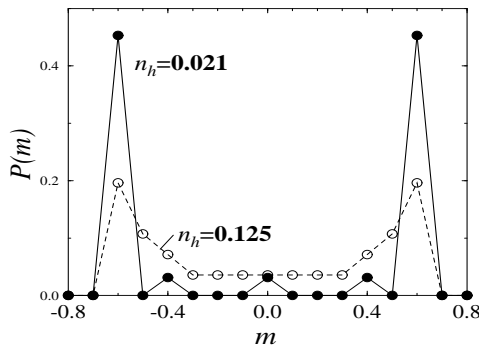


Fig. 8. The distribution function of the magnetic moment, $P(m)$, for $n_h = 1/48 = 0.021$ (●) and for $n_h = 1/8 = 0.125$ (○) in VIC, which correspond to the cases of Figs. 5(a) and 5(b), respectively. Lines are guides for the eye.

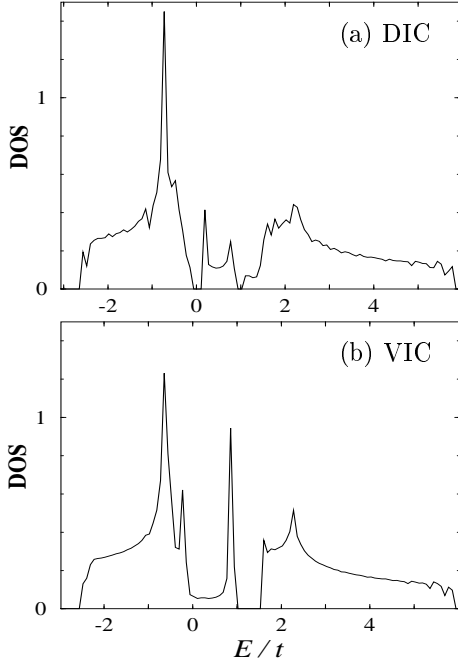


Fig. 9. The density of states $N(E)$. $U = 3.6t$, $t'/t = -1/6$, $n_h = 1/16 = 0.0625$. (a) The insulator DIC case of Fig. 1(b). $\delta/n_h = 1/2$. (b) The metallic VIC case of Fig. 2(c). $\delta/n_h = 3/4$. The Fermi energy E_F is at 0.

or μSR) changes its shape reflecting the change from the square wave to the sinusoidal wave. At smaller n_h , $P(m)$ splits into two sharp peaks around $\pm \max|m_i|$ as in the AF state. At large n_h , $P(m)$ distributes broadly between the two peaks.

As for the profile of the charge density, in the limit of large n_h , $n_2\mathbf{Q}/m\mathbf{Q}$ is finite and other $n_l\mathbf{Q} \rightarrow 0$ ($l \geq 4$). It means that n_i is reduced to the simple sinusoidal wave with half period of m_i . In the limit of small n_h , $n_l\mathbf{Q} \sim -(-1)^{l/2}n_h \rightarrow 0$ ($l \geq 2$: even integer). It reflects that the excess carriers are restricted in the δ -function-like stripe region whose width is a few sites, and that the other wide region is the insulating half-filled AF state.

The spatial profile of the stripe structure obtained here is qualitatively the same as that of the insulator state at $t' = 0$.^{15,16,18)} Our results show that the solitonic

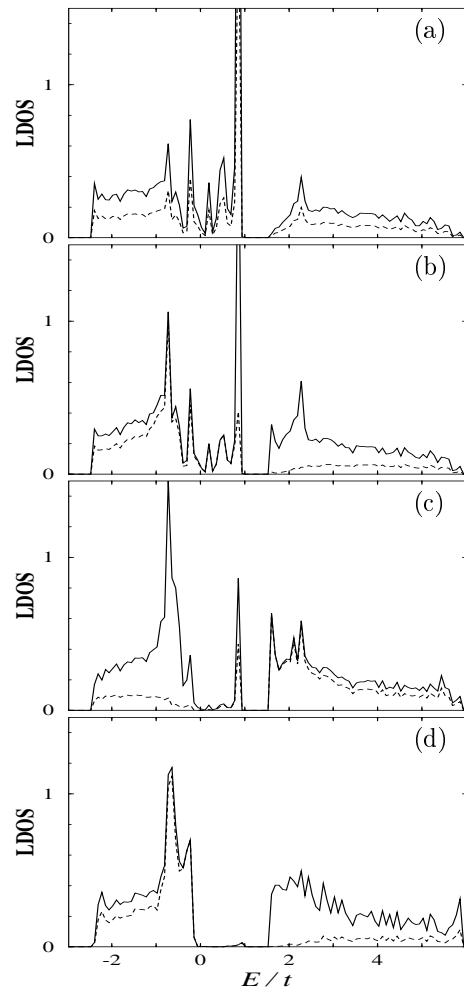


Fig. 10. Local density of states $N(\mathbf{r}, E)$ in the metallic VIC case of Fig. 9(b). (a) At the center site of the stripe. (b) At the nearest neighbor site to the center site. (c) At the next nearest neighbor site to the center site. (d) At the farthest site from the stripe. With leaving the stripe [(a) to (d)], the contribution from the mid-gap state disappears. Dashed lines show the up-spin contribution. $U = 3.6t$, $t'/t = -1/6$, $n_h = 1/16 = 0.0625$, $\delta/n_h = 3/4$. The Fermi energy E_F is at 0.

profile in the insulator state remains unchanged even in the metallic state. But the electronic state is changed in the metallic state. We discuss it in the following sections.

§4. Local Density of States

In terms of the eigen-energy and the wave-function, Green's function can be written as

$$G_\sigma(\mathbf{r}, \mathbf{r}', E) = \sum_{\mathbf{k}_0, \alpha} \frac{u_{\mathbf{k}_0, \sigma, \alpha}(\mathbf{r}) u_{\mathbf{k}_0, \sigma, \alpha}^*(\mathbf{r}')}{E + i\eta - E_{\mathbf{k}_0, \sigma, \alpha}}, \quad (4.1)$$

where

$$u_{\mathbf{k}_0, \sigma, \alpha}(\mathbf{r}_i) = N_k^{-1/2} \sum_m e^{i(\mathbf{k}_0 + m\mathbf{Q}) \cdot \mathbf{r}_i} u_{\mathbf{k}_0, \sigma, \alpha, m} \quad (4.2)$$

and $\eta(> 0)$ is an infinitesimally small constant. We obtain the LDOS by

$$N_\sigma(\mathbf{r}_i, E) = -\frac{1}{\pi} \text{Im} G_\sigma(\mathbf{r}_i, \mathbf{r}_i, E)$$

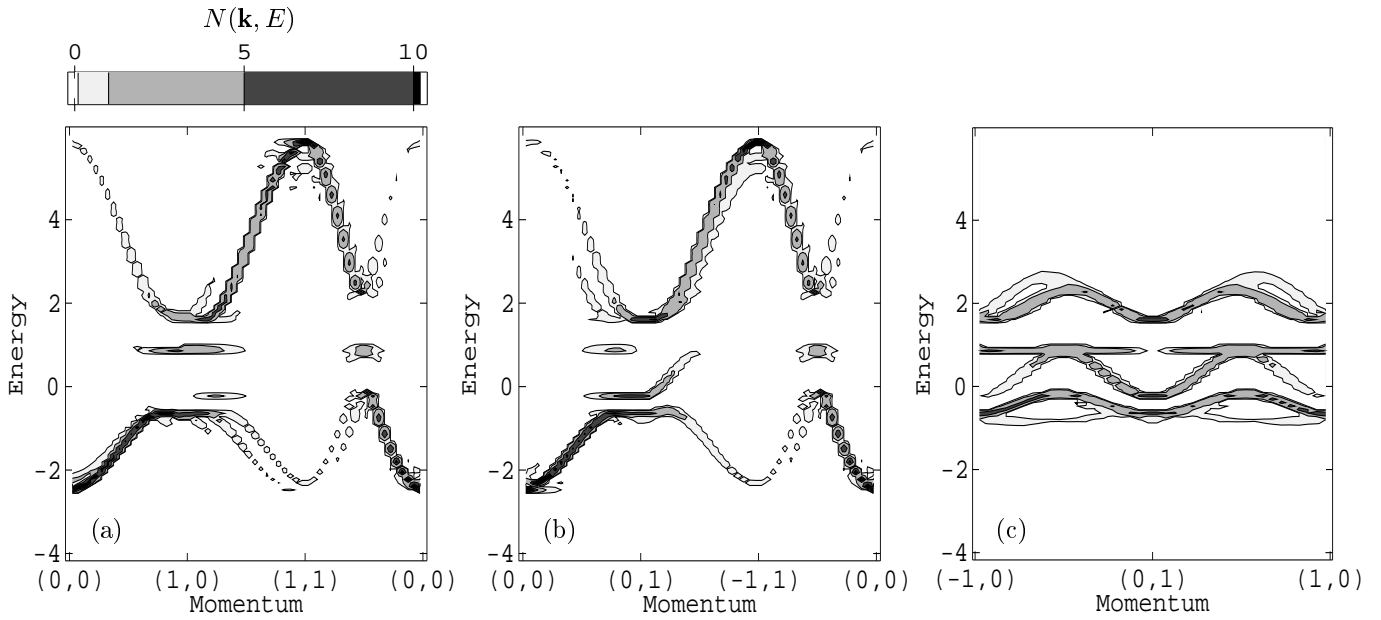


Fig. 11. Contour map of the spectral weight $N(\mathbf{k}, E)$ along the symmetry lines in the original Brillouin zone for the metallic VIC case of Fig. 2(c). (a) Along the line $(0,0) - (1,0) - (1,1) - (0,0)$ in reciprocal lattice units. (b) Along the line $(0,0) - (0,1) - (-1,1) - (0,0)$. (c) Along the line $(-1,0) - (0,1) - (1,0)$. $U = 3.6t$, $t'/t = -1/6$, $n_h = 1/16 = 0.0625$, $\delta/n_h = 3/4$. The Fermi energy E_F is at 0. Energy E is scaled by t .

$$= \sum_{\mathbf{k}_0, \alpha} |u_{\mathbf{k}_0, \sigma, \alpha}(\mathbf{r}_i)|^2 \delta(E - E_{\mathbf{k}_0, \sigma, \alpha}). \quad (4.3)$$

The DOS is the spatial average of LDOS, i.e.,

$$N_\sigma(E) = N_k^{-1} \sum_i N_\sigma(\mathbf{r}_i, E) = N_k^{-1} \sum_{\mathbf{k}_0, \alpha} \delta(E - E_{\mathbf{k}_0, \sigma, \alpha}). \quad (4.4)$$

Figure 9 shows the DOS for DIC and VIC in the case $n_h = 1/16 = 0.0625$. The mid-gap state is seen within the large AF gap. In the insulator DIC case, there is a small gap between the mid-gap states and the valence band, and E_F is located in the small gap. In the metallic VIC case, the small gap is buried in this DOS plot. For the case $\delta = \frac{1}{2}n_h$, $E_F (= 0)$ is located at the overlapped mid-gap state and the valence band. With increasing δ at fixed n_h , E_F is shifted to higher energy without qualitative change of the DOS structure. But, in the large $\delta (\sim n_h)$ case for large $n_h (\geq 0.1)$, the mid-gap state and the valence band are separated in the DOS plot, where E_F is located in the mid-gap states. As a result, even in the metallic state, a gap feature in the electron state still remains. This point is discussed further in the next section.

Next, we consider the LDOS, $N(\mathbf{r}_i, E)$. It is shown in Fig. 10. The contribution of the mid-gap state is enhanced at the center of the stripe, and decreased with leaving the center. Far from the stripe, the LDOS is like an AF-gapped spectrum since the mid-gap state's contribution vanishes. For $\delta = \frac{3}{4}n_h$ (and also for $\delta = n_h$), E_F located in the mid-gap state is in the AF gap outside the stripe region [Fig. 10(d)]. Then only the stripe region is metallic, and the other AF region is an insulator. If $\delta = \frac{1}{2}n_h$ in the metallic VIC case, where E_F is effectively

shifted to lower energy, E_F touches the mid-gap state in the stripe region and the valence band in the outside region. Then, both the stripe region and outer AF region are metallic. If these characteristic features of the \mathbf{r} -resolved DOS structure are observed by experiments such as STM, it may be a powerful means to confirm the solitonic features of the stripe structure.

§5. Spectral Weight

In this section, we study the \mathbf{k} -resolved DOS, i.e., spectral weight at each \mathbf{k} point. It is given by

$$\begin{aligned} N_\sigma(\mathbf{k}, E) &= -\frac{1}{\pi} \text{Im} G_\sigma(\mathbf{k}, E) \\ &= \sum_{\mathbf{k}_0, \alpha, m} |u_{\mathbf{k}_0, \sigma, \alpha, m}|^2 \delta(E - E_{\mathbf{k}_0, \sigma, \alpha}) \delta(\mathbf{k}_0 + m\mathbf{Q} - \mathbf{k}), \end{aligned} \quad (5.1)$$

where

$$G_\sigma(\mathbf{k}, E) = N_k^{-1} \sum_{\mathbf{r}, \mathbf{r}'} e^{-i\mathbf{k} \cdot (\mathbf{r} - \mathbf{r}')} G_\sigma(\mathbf{r}, \mathbf{r}', E). \quad (5.2)$$

In eq. (5.1), the momentum of the center of mass coordinate $(\mathbf{r} + \mathbf{r}')/2$ is set to be 0, since we consider the spatial average.

First, we consider the VIC case of Fig. 2(c) for $n_h = 1/16 = 0.0625$ and $\delta = \frac{3}{4}n_h$. Figures 11 shows the contour map of $N(\mathbf{k}, E) = \sum_\sigma N_\sigma(\mathbf{k}, E)$ along the symmetry lines in the original Brillouin zone. We also calculate $N(\mathbf{k}, E)$ for other n_h cases, and obtain qualitatively the same structure. While the energy dispersion splits into N -bands by the N -site periodicity, the spectral weight in $2\pi \times 2\pi$ \mathbf{k} -space has the structure re-

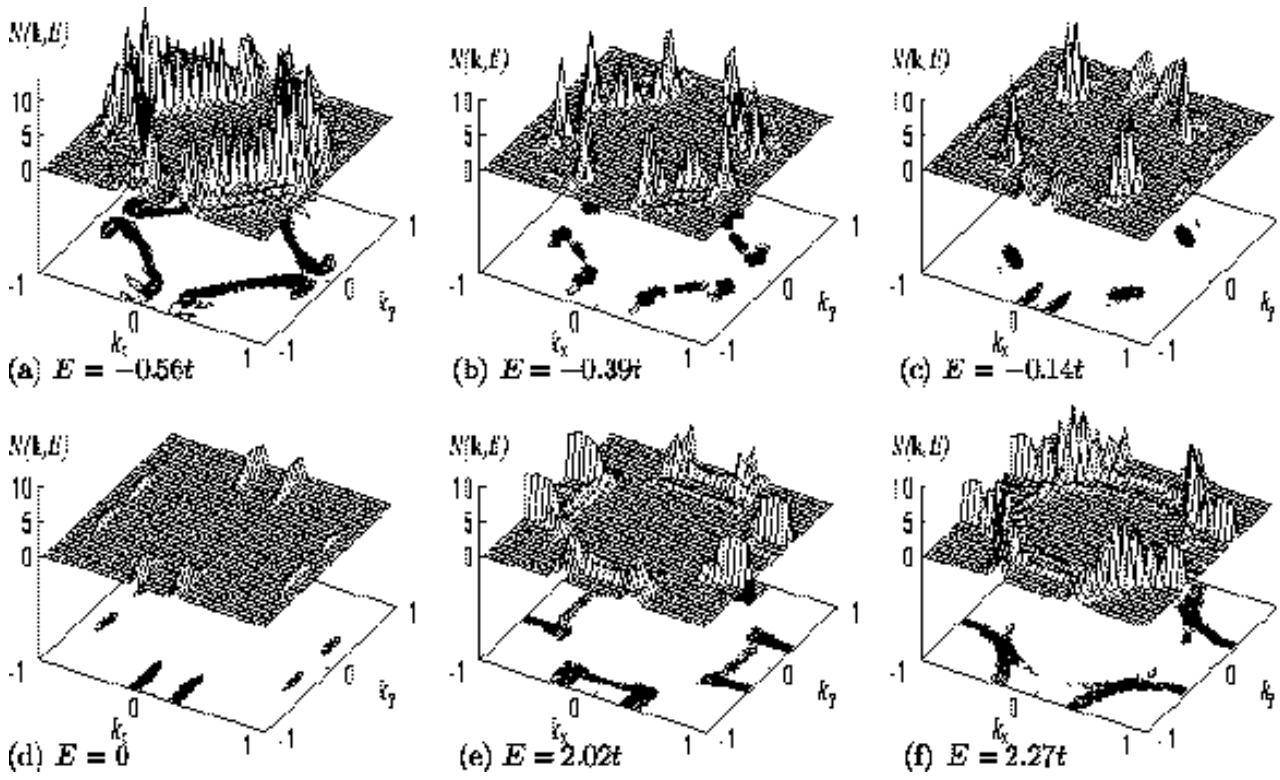


Fig. 12. Spectral weight $N(\mathbf{k}, E)$ in $2\pi \times 2\pi$ \mathbf{k} -space at fixed E in the VIC case of Fig. 11. $E/t = -0.56$ (a), -0.39 (b), -0.14 (c), 0 (d), 2.02 (e), 2.27 (f). We see the valence band in (a)-(c), the mid-gap state in (c) and (d), the conduction band in (e) and (f). k_x and k_y are scaled by π . $U = 3.6t$, $t'/t = -1/6$, $n_h = 1/16 = 0.0625$, $\delta/n_h = 3/4$. The Fermi surface for $\delta/n_h = 3/4$ corresponds to the ridges in (d). The Fermi surface for $\delta/n_h = 1/2$ has the same structure as the ridges in (c).

flecting the original dispersion $\epsilon(\mathbf{k})$ as shown in Fig. 11, since the amplitude of the wave function $u_{\mathbf{k}_0, \sigma, \alpha, m}$ for each m reflects the original dispersion $\epsilon(\mathbf{k})$. Some mQ -shifted $\epsilon(\mathbf{k})$ by the band folding also appear in the figure. While their amplitude are usually small, they form the SDW gap and the mid-gap states. Darker region in Fig. 11 means larger $N(\mathbf{k}, E)$. As the stripe is a 1D structure, $N(\mathbf{k}, E)$ is two-fold symmetric. Then, there are differences of $N(\mathbf{k}, E)$ between $(1, 0)$ and $(0, 1)$ directions in the VIC case. In Fig. 11, $N(\mathbf{k}, E = E_F)$ has little amplitude around $(1, 0)$. But near $(0, 1)$, the mid-gap state appears with large amplitude at E_F . There, we can see the split of the mid-gap state and the valence band below E_F . Around $(\frac{1}{2}, \frac{1}{2})$ and $(-\frac{1}{2}, \frac{1}{2})$, we see a gapped structure, where the mid-gap state does not appear at E_F .

These features of the spectral weight are consistent with those obtained by the ARPES experiments on LSCO.^{26, 27, 28)} Since there are two-type domains of the x -direction and the y -direction stripe in the material, we observe the spectral weight as $N_D(\mathbf{k}, E) = [N(\mathbf{k}, E) + N(k_x \leftrightarrow k_y, E)]/2$, i.e., the overlap of $N(\mathbf{k}, E)$ in Figs. 11(a) and 11(b).

When δ is shifted keeping n_h fixed, we confirm that $N(\mathbf{k}, E)$ is not qualitatively changed except for the position of E_F . With increasing δ , E_F is shifted to upper energy. For larger δ such as $\delta = n_h$, the gap edge at $(\frac{1}{2}, \frac{1}{2})$ is located at deeper position below E_F . The ARPES

experiments^{26, 27, 28)} reported that the gap at $(\frac{1}{2}, \frac{1}{2})$ for $x = 0.15$ disappears with increasing n_h . This gap disappearance can be explained as follows in our scenario. In the elastic neutron scattering data,^{6, 7, 8, 9)} with increasing n_h , δ shows saturation and it is shifted from $\delta \sim n_h$ to $\delta \sim \frac{1}{2}n_h$. When δ approaches $\frac{1}{2}n_h$, E_F is effectively shifted toward lower energy, and touches the top of the valence band near $(\frac{1}{2}, \frac{1}{2})$. Then, the gap in the $(\frac{1}{2}, \frac{1}{2})$ -direction disappears. As E_F approaches the gap-edge at $(\frac{1}{2}, \frac{1}{2})$ gradually, the gap disappearance is “observed” at larger δ than $\delta = \frac{1}{2}n_h$, if the energy resolution is broad in the experiment.

To clearly see the \mathbf{k} -dependent SDW gap, we consider $N(\mathbf{k}, E)$ in $2\pi \times 2\pi$ \mathbf{k} -space at fixed E . It is shown in Fig. 12 for VIC. From (a) to (f), E is increased. In Figs. 12(a)-(c), the valence band appears. Its behavior is understood by considering $E_-(\mathbf{k})$ of the C-AF case in eq. (3.1). Below E_F , $N(\mathbf{k}, E)$ has ridges along the contour line for $E = E_-(\mathbf{k})$. Far from E_F , it reflects the original dispersion $\epsilon(\mathbf{k})$ [Fig. 12(a)]. For $E_-(\pi(1, 0)) < E < E_-(\pi(\frac{1}{2}, \frac{1}{2}))$, $N(\mathbf{k}, E)$ disappears near $(1, 0)$ and $(0, 1)$, because the AF gap opens at these \mathbf{k} -points. With increasing E , the remained contour lines of $E_-(\mathbf{k})$ decrease their length, and converge upon $(\frac{1}{2}, \frac{1}{2})$ [Figs. 12(b) and 12(c)]. Near E_F , we also see the fragmentation of the ridges due to the x -direction 1D stripe structure [Figs. 12(b)]. The valence band contribution disappears for $E > E_-(\pi(\frac{1}{2}, \frac{1}{2}))$.

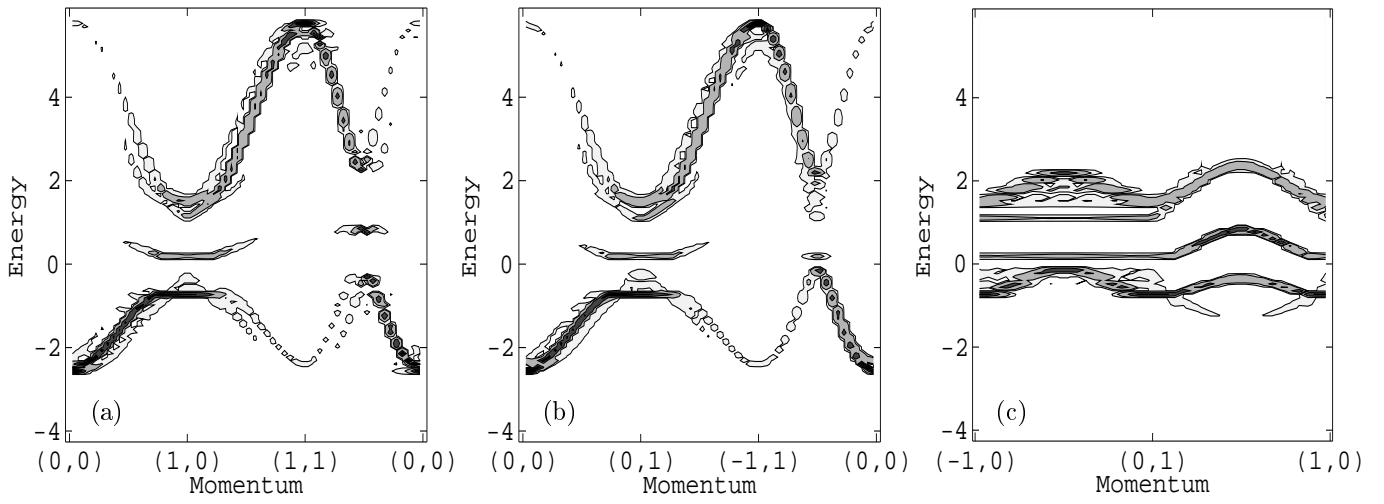


Fig. 13. The same as Fig. 11, but for the insulator DIC case of Fig. 1(b). $U = 3.6t$, $t'/t = -1/6$, $n_h = 1/16 = 0.0625$, $\delta/n_h = 1/2$.

The mid-gap state appears in Fig. 12(c) and 12(d). On raising E , it first appears near $(0, 1)$ [and $(1, 0)$ with small amplitude] at the bottom of the mid-gap bands in addition to the valence band contribution [Figs. 12(c)]. The “Fermi surface” in the VIC case corresponds to the ridges shown in Fig. 12(d), where the valence band contribution already disappears. Since the mid-gap state is localized along the x -directional stripe, $N(\mathbf{k}, E)$ is distributed on lines perpendicular to k_x direction, like a 1D Fermi surface. As it also reflects the original Fermi surface of $\epsilon(\mathbf{k})$, the amplitude of $N(\mathbf{k}, E)$ is large near $(0, 1)$. Then in the spectral weight of the domain structure $N_D(\mathbf{k}, E)$, the Fermi surface exists near $(0, 1)$ and $(1, 0)$, but disappears near $(\frac{1}{2}, \frac{1}{2})$. This \mathbf{k} -dependent Fermi surface structure is consistent with the ARPES results.^{27, 28)} We obtain qualitatively the same Fermi surface also for $\delta = n_h$. It is qualitatively the same results of the case $t' = 0$ under the test stripe potential in ref. 21. For $\delta = \frac{1}{2}n_h$, since E_F is decreased effectively, the Fermi surface has the same structure as shown in Fig. 12(c), i.e., the valence band contribution also appears near $(\frac{1}{2}, \frac{1}{2})$ in addition to the mid-gap state’s contribution near $(1, 0)$. This feature is contrasted with the $\delta = \frac{3}{4}n_h$ case as mentioned above.

With increasing E , the larger ridge-wall near $(0, 1)$ shown in Fig. 12(d) goes away from the line $k_x = 0$, and the small ridge-wall near $(1, 0)$ approaches $k_x = 0$. In this shift, the ridge of $N(\mathbf{k}, E)$ has large peaks near the \mathbf{k} -points of the original Fermi surface by $\epsilon(\mathbf{k})$. Then, if δ is randomly distributed (it means effectively that E_F is randomly distributed), the original Fermi surface shape of $\epsilon(\mathbf{k})$ appears as an average.²¹⁾

The conduction band contribution appears in Figs. 12(e) and 12(f). It qualitatively follows $E_+(\mathbf{k})$ dispersion in eq. (3.1). For $E_+(\pi(1, 0)) < E < E_+(\pi(\frac{1}{2}, \frac{1}{2}))$, the conduction band contribution appears only near $(1, 0)$ and $(0, 1)$ [Fig. 12(e)]. With increasing E , it spreads and approaches $(\frac{1}{2}, \frac{1}{2})$, and it is connected each other. For $E > E_+(\pi(\frac{1}{2}, \frac{1}{2}))$, the ridges of $N(\mathbf{k}, E)$ reflect the original dispersion $\epsilon(\mathbf{k})$. We also see the small amplitude

of the circle ridge around $(0, 0)$, which is the \mathbf{Q} -shift of the original $\epsilon(\mathbf{k})$ contribution.

Next, we consider the DIC case calculated for the same parameter set. It is shown in Figs. 13 and 14. There, $l\mathbf{Q}$ -shifted $\epsilon(\mathbf{k})$ dispersion curves form the valence band, the conduction band and the mid-gap state as in the VIC case. As shown in Fig. 13, a small gap opens between the valence band and the mid-gap state in the DIC case, and E_F is in the gap. Reflecting the diagonal-direction stripe, $N(\mathbf{k}, E)$ is two-fold symmetric. The differences appear between the $(\frac{1}{2}, \frac{1}{2})$ -direction and the $(-\frac{1}{2}, \frac{1}{2})$ -direction. In Fig. 13(c), $N(\mathbf{k}, E)$ shows flat dispersion near E_F along the line $(-1, 0) - (0, 1)$. It reflects the 1D-like dispersion due to the stripe, as discussed below.

To clearly see the \mathbf{k} -dependent SDW gap for DIC, we consider $N(\mathbf{k}, E)$ at fixed E as shown in Fig. 14. The valence band contribution appears in Figs. 14(a)-(c). For $E_-(\pi(1, 0)) < E < E_-(\pi(\frac{1}{2}, \frac{1}{2}))$, $N(\mathbf{k}, E)$ near $(1, 0)$ and $(0, 1)$ disappears as in the VIC case. Further, by the effect of the diagonal stripe, the remained ridge-wall near $(\frac{1}{2}, \frac{1}{2})$ is split into two peaks [Fig. 14(a)], and shifted toward $(\frac{1}{2}, \frac{1}{2})$ [Fig. 14(b)], and disappears [Fig. 14(c)], with increasing E . As for the ridge-wall near $(-\frac{1}{2}, \frac{1}{2})$, its length monotonically shrinks on raising E [Figs. 14(a) and 14(b)], but the ridge survives for a while after the $(\frac{1}{2}, \frac{1}{2})$ -ridge disappears [Fig. 14(c)].

Figure 14(d) shows the mid-gap state’s contribution. As the mid-gap state is localized along the diagonal stripe, its dispersion is 1D-like. The ridge-wall approaches the line $k_x = k_y$ with increasing E . The ridge-wall has two large peaks. Their peak-positions are near the contour line of the original dispersion $\epsilon(\mathbf{k})$.

The conduction band contribution appears in Figs. 14(e) and 14(f). At the bottom of the conduction band, the peaks of $N(\mathbf{k}, E)$ appear around $(1, 0)$ and $(0, 1)$ [Fig. 14(e)]. And the additional ridges connect these peaks along the line $(1, 0) - (0, -1)$. The peaks are separated along the $(1, 0) - (0, 1)$ direction. This 1D-like ridge comes from the diagonal stripe structure. With increas-

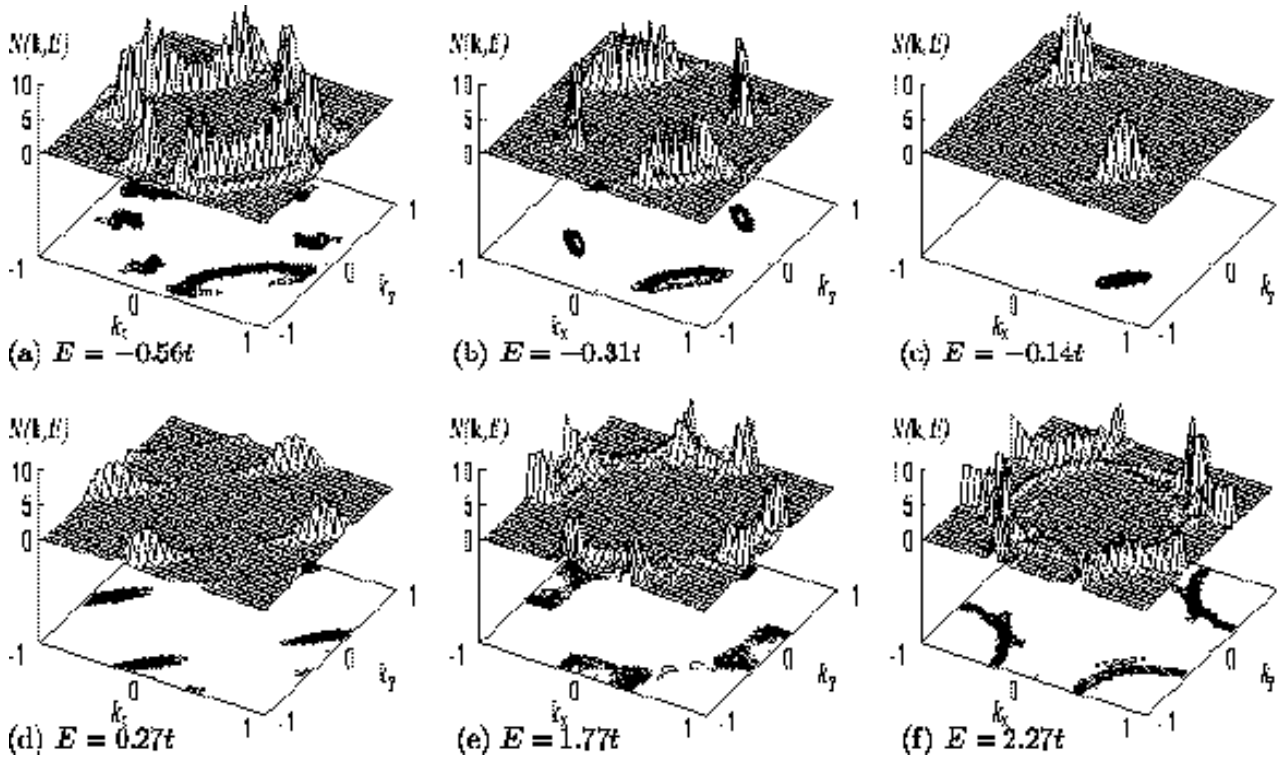


Fig. 14. Spectral weight $N(\mathbf{k}, E)$ in $2\pi \times 2\pi$ \mathbf{k} -space at fixed E in the DIC case of Fig. 13. $E/t = -0.56$ (a), -0.31 (b), -0.14 (c), 0.27 (d), 1.77 (e), 2.27 (f). We see the valence band in (a)-(c), the mid-gap state in (d), the conduction band in (e) and (f). k_x and k_y are scaled by π . $U = 3.6t$, $t'/t = -1/6$, $n_h = 1/16 = 0.0625$, $\delta/n_h = 1/2$.

ing E , the contributions near $(1, 0)$ and $(0, 1)$ spread out, and they are connected each other. Then, $N(\mathbf{k}, E)$ has a connected ridge along the contour line of the original dispersion $\epsilon(\mathbf{k})$ [Fig. 14(f)]. We also see the \mathbf{Q} -shifted contribution of $\epsilon(\mathbf{k})$ as small ridges.

§6. Optical Conductivity

We calculate the optical conductivity by the inter-band vertical transition within the reduced Brillouin zone. Since there are N bands in the stripe structure as shown in Figs. 1 and 2, the inter-band absorption occurs by these N bands. The optical conductivity $\text{Re}\sigma_{j,j'}(\omega)$ ($j, j' = x, y$) is given by the Kubo-Greenwood formula.^{39,40,41} In our notation, it is written as

$$\begin{aligned} \text{Re}\sigma_{j,j'}(\omega) &= \frac{\pi}{\omega N_k} \sum_{\mathbf{k}_0, \alpha, \alpha', \sigma} f(E_{\mathbf{k}_0, \alpha, \sigma}) [1 - f(E_{\mathbf{k}_0, \alpha', \sigma})] \\ &\times \langle \mathbf{k}_0, \alpha, \sigma | J_j | \mathbf{k}_0, \alpha', \sigma \rangle \langle \mathbf{k}_0, \alpha, \sigma | J_{j'} | \mathbf{k}_0, \alpha', \sigma \rangle \\ &\times [\delta(E_{\mathbf{k}_0, \alpha, \sigma} - E_{\mathbf{k}_0, \alpha', \sigma} + \omega) - \delta(E_{\mathbf{k}_0, \alpha, \sigma} - E_{\mathbf{k}_0, \alpha', \sigma} - \omega)]. \end{aligned} \quad (6.1)$$

Equation (6.1) is derived from the current-current correlation function. The x -component of the current operator is defined as $\hat{J}_x(\mathbf{r}_i) = -ie|\epsilon| \sum_{\sigma} \{t(a_{i+\hat{x}, \sigma}^\dagger - a_{i-\hat{x}, \sigma}^\dagger) + t'(a_{i+\hat{x}+\hat{y}, \sigma}^\dagger + a_{i+\hat{x}-\hat{y}, \sigma}^\dagger - a_{i-\hat{x}+\hat{y}, \sigma}^\dagger - a_{i-\hat{x}-\hat{y}, \sigma}^\dagger)\} a_{i, \sigma}$ in our square lattice case, where $i+\hat{x}$ and $i+\hat{y}$ mean (i_x+1, i_y)

and (i_x, i_y+1) , respectively. Then, the x -component of the oscillator strength in eq. (6.1) is given by

$$\begin{aligned} \langle \mathbf{k}_0, \alpha, \sigma | J_x | \mathbf{k}_0, \alpha', \sigma \rangle &= |e| \sum_i [t\{u_{\mathbf{k}_0, \alpha, \sigma}(\mathbf{r}_{i+\hat{x}}) \\ &- u_{\mathbf{k}_0, \alpha, \sigma}(\mathbf{r}_{i-\hat{x}})\} + t'\{u_{\mathbf{k}_0, \alpha, \sigma}(\mathbf{r}_{i+\hat{x}+\hat{y}}) + u_{\mathbf{k}_0, \alpha, \sigma}(\mathbf{r}_{i+\hat{x}-\hat{y}}) \\ &- u_{\mathbf{k}_0, \alpha, \sigma}(\mathbf{r}_{i-\hat{x}+\hat{y}}) - u_{\mathbf{k}_0, \alpha, \sigma}(\mathbf{r}_{i-\hat{x}-\hat{y}})\}\} u_{\mathbf{k}_0, \alpha', \sigma}(\mathbf{r}_i)] \end{aligned} \quad (6.2)$$

instead of the usual form $\langle \psi_{\mathbf{k}} | \nabla_x | \psi_{\mathbf{k}'} \rangle$.

Figure 15 shows $\text{Re}\sigma_{\parallel}(\omega)$ for the parallel field to the stripe and $\text{Re}\sigma_{\perp}(\omega)$ for the perpendicular field in the VIC case. Here, we do not consider the Drude absorption by the intra-band inelastic scattering. For $n_h = 1/26 = 0.0385$ [Fig. 15(a)], there is a large peak near $\omega \sim 2.5t$. It comes from the valence band \rightarrow conduction band absorption with larger ω than the AF gap, and survives also in the C-AF state. We call the peak as the “AF peak”. The peaks at $\omega/t = 1 \sim 1.5$ comes from the absorption related to the mid-gap states. We call them as the “mid-gap peaks”. They vanish in the C-AF state. For larger n_h [Fig. 15(b)], the AF peak is suppressed and the mid-gap peaks are enhanced. The mid-gap peaks of $\text{Re}\sigma_{\perp}(\omega)$ are slightly shifted to lower ω compared with $\text{Re}\sigma_{\parallel}(\omega)$.

The DIC case is shown in Fig. 16. With increasing n_h , the AF peak is suppressed and the mid-gap peaks are enhanced, as in the VIC case. There are large differences

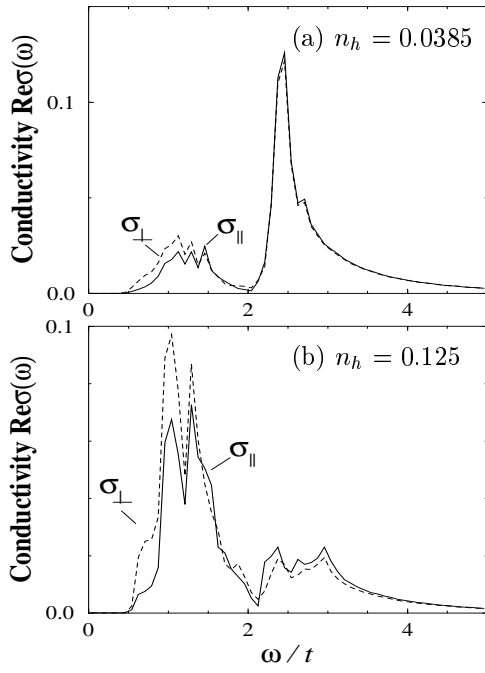


Fig. 15. Optical conductivity $\text{Re}\sigma_{||}(\omega)$ [solid lines] and $\text{Re}\sigma_{\perp}(\omega)$ [dashed lines] for VIC in an arbitrary unit. $\text{Re}\sigma_{||}(\omega)$ ($\text{Re}\sigma_{\perp}(\omega)$) is for the field parallel (perpendicular) to the stripe. The Drude absorption is not included in this figure. (a) $n_h = 1/26 = 0.0385$, $\delta/n_h = 13/18$. (b) $n_h = 1/8 = 0.125$, $\delta/n_h = 5/7$. $U = 3.6t$, $t'/t = -1/6$.

between $\text{Re}\sigma_{||}(\omega)$ and $\text{Re}\sigma_{\perp}(\omega)$ in the DIC case. The mid-gap peaks of $\text{Re}\sigma_{\perp}(\omega)$ are large, and they are located at larger ω . For $n_h = 1/8 = 0.125$, the AF peak vanishes for $\text{Re}\sigma_{\perp}(\omega)$, but still has large height for $\text{Re}\sigma_{||}(\omega)$.

The experiments of the optical conductivity were performed on LSCO [ref. 30] and $\text{La}_{2-x}\text{Sr}_x\text{NiO}_4$ [ref. 31]. There, the broad peak develops in the mid-infrared region with increasing n_h . It may be related to the mid-gap peak's contribution of the stripe state.

§7. Summary and Discussions

The stripe structure in high- T_c cuprates and its electronic structure are studied by the self-consistent mean-field theory of the Hubbard model. The SDW gapped insulator is changed to a metal by introducing the realistic Fermi surface topology in VIC. For appropriate U , DIC is changed to VIC at critical n_h with increasing n_h . The DIC is insulator, and VIC can be metallic. In the insulator, $\delta = \frac{1}{2}n_h$. But, in the metallic VIC, δ can be larger than $\frac{1}{2}n_h$. These features seem to be consistent with the experimental results of the elastic neutron scattering,^{6,7,8,9,10,11,12} as discussed in §3.

The SDW and CDW of the stripe structure are a sinusoidal wave at large n_h . They become, respectively, square and solitonic waves at small n_h . There, excess carriers are localized in the stripe region and the outer region is half-filled AF. The localized state forms the mid-gap state inside the AF gap. We calculate the LDOS, the spectral weight and the optical conductivity, and clarify the contribution of the mid-gap state. In the metallic VIC case, only the mid-gap state appears at E_F for

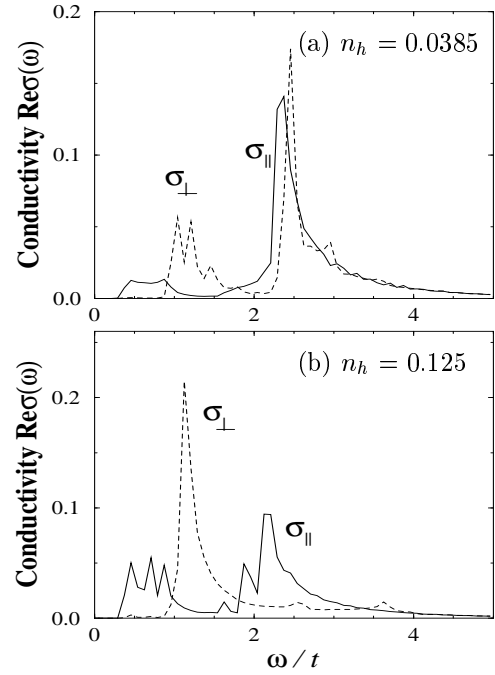


Fig. 16. Optical conductivity $\text{Re}\sigma_{||}(\omega)$ [solid lines] and $\text{Re}\sigma_{\perp}(\omega)$ [dashed lines] for DIC in an arbitrary unit. (a) $n_h = 1/26 = 0.0385$. (b) $n_h = 1/8 = 0.125$. $U = 3.6t$, $t'/t = -1/6$, $\delta/n_h = 1/2$.

$\delta/n_h \sim \frac{3}{4}$ or larger. Then, while the stripe region is metallic locally in space, the outer AF region is an insulator. Metallicity attains locally on the stripe region for finite n_h . In the spectral weight, the contribution of the mid-gap state has large amplitude near $(0, 1)$ and little amplitude near $(\frac{1}{2}, \frac{1}{2})$ at E_F in VIC. Then, the “Fermi surface” disappears near $(\frac{1}{2}, \frac{1}{2})$, leaving the Fermi surface “arcs”. On the other hand, for $\delta/n_h \sim \frac{1}{2}$, both the mid-gap state and the valence band appear at E_F . In this case, both the inside and outside spatial regions of the stripe are metallic. In the spectral weight, the valence band contribution appears near $(\frac{1}{2}, \frac{1}{2})$ in addition to the mid-gap state's contribution near $(0, 1)$. Then, the Fermi surface is observed as a connected one. These features of the spectral weight are consistent with the ARPES experiments,^{26,27,28} as discussed in §5. As a result, the electronic structure near E_F is determined by the ratio of the incommensurability and the hole density, δ/n_h , which is a key parameter of the problem. We expect that the features of the electronic state obtained here are examined by the experiments such as ARPES, STM and the optical conductivity. These experiments may be powerful methods to obtain vital information about the mechanism of the stripe structure in high- T_c cuprates.

So far, the metallic stripe state with $\delta/n_h \sim 1$ could not be reproduced by the mean field theory, which gives an insulator with $\delta/n_h = \frac{1}{2}$. Then, the stripe state was said to be an anomalous state where the mean field theory can not be applied. However, by introducing the realistic Fermi surface topology, the mean field theory can give the metallic state with $\delta/n_h = 0.75 \sim 0.88$ (which approaches 1 depending on the Fermi surface topology) even in a simple Hubbard model. While the mean field

theory over-estimates the stable parameter region of the ordered states or the AF moments, the obtained features are qualitatively valid as a first approximation within the ordered state. Then, the mean-field theory can be a first step for further studies to consider the effects of the extra interactions or fluctuations, and to obtain the behavior of the various physical quantities in the stripe state.

-
- [1] K. Machida and M. Fujita: Phys. Rev. B **30** (1984) 5284.
 - [2] For a review, E. Fawcett: Rev. Mod. Phys. **60** (1988) 209.
 - [3] M. Fujita and K. Machida: J. Phys. C **21** (1988) 5813.
 - [4] Y. Fagot-Revurat, M. Horvatić, C. Berthier, P. Ségransan, G. Dhalenne and A. Revcolevschi: Phys. Rev. Lett. **77** (1996) 1861.
 - [5] V. Kiryukhin, B. Keimer, J.P. Hill and A. Vigliante: Phys. Rev. Lett. **76** (1996) 4608.
 - [6] S. Wakimoto, G. Shirane, Y. Endoh, K. Hirota, S. Ueki, K. Yamada, R.J. Birgeneau, M.A. Kastner, Y.S. Lee, P.M. Gehring and S.H. Lee: Phys. Rev. B **60** (1999) 769.
 - [7] S. Wakimoto, K. Yamada, S. Ueki, G. Shirane, Y.S. Lee, S.H. Lee, M.A. Kastner, K. Hirota, P.M. Gehring, Y. Endoh and R.J. Birgeneau: cond-mat/9902319.
 - [8] T. Suzuki, T. Goto, K. Chiba, T. Shinoda, T. Fukase, H. Kimura, K. Yamada, M. Ohashi and Y. Yamaguchi: Phys. Rev. B **57** (1998) R3229, and earlier references cited therein.
 - [9] For a review, see J.M. Tranquada: in *Neutron Scattering in Layered Copper-Oxide Superconductors*, edited by A. Furrer (Kluwer, Dordrecht, The Netherlands, 1998), pp.225-260; J. Phys. Chem. Solids **59** (1998) 2150.
 - [10] J.M. Tranquada, J.D. Axe, N. Ichikawa, A.R. Moodenbaugh, Y. Nakamura and S. Uchida: Phys. Rev. Lett. **78** (1997) 338, and earlier references cited therein.
 - [11] J.M. Tranquada, D.J. Buttrey and V. Sachan: Phys. Rev. B **54** (1996) 12318, and earlier references cited therein.
 - [12] H. Yoshizawa, T. Kakeshita, R. Kajimoto, T. Tanabe, T. Katsumuji and Y. Tokura: Physica B **241-243** (1998) 880.
 - [13] H.A. Mook, P. Dai, S.M. Hayden, G. Aeppli, T.G. Perring and F. Doğan: Nature **395** (1998) 580. H.A. Mook, F. Doğan and B. C. Chakoumakos: cond-mat/9811100.
 - [14] M. Arai, T. Nishijima, Y. Endoh, T. Egami, S. Tajima, K. Tomimoto, Y. Shinohara, M. Takahashi, A. Garrett and S.M. Bennington: Phys. Rev. Lett. **83** (1999) 608.
 - [15] K. Machida: Physica C **158** (1989) 192.
 - [16] M. Kato, K. Machida, H. Nakanishi and M. Fujita: J. Phys. Soc. Jpn. **59** (1990) 1047.
 - [17] D. Poilblanc and T.M. Rice: Phys. Rev. B **39** (1989) 9749.
 - [18] J. Zaanen and O. Gunnarsson: Phys. Rev. B **40** (1990) 7391.
 - [19] H. Schulz: Phys. Rev. Lett. **64** (1990) 1445.
 - [20] J. Zaanen and A.M. Oleś: Ann. Phys. **5** (1996) 224.
 - [21] M.I. Salkola, V.J. Emery and S.A. Kivelson: Phys. Rev. Lett. **77** (1996) 155.
 - [22] S. White and D. Scalapino: Phys. Rev. Lett. **80** (1998) 1272.
 - [23] See for example, V.J. Emery, S.A. Kivelson and O. Zachar: Phys. Rev. B **56** (1997) 6120.
 - [24] T. Mizokawa and A. Fujimori: Phys. Rev. Lett. **80** (1998) 1320; Phys. Rev. B **56** (1997) 11920.
 - [25] F. Ronning, C. Kim, D.L. Feng, D.S. Marshall, A.G. Loeser, L.L. Miller, J.N. Eckstein, I. Bozovic and Z.-X. Shen: Science **282** (1998) 2068.
 - [26] A. Ino, T. Mizokawa, K. Kobayashi, A. Fujimori, T. Sasagawa, T. Kimura, K. Kishio, K. Tamasaku, H. Eisaki and S. Uchida: Phys. Rev. Lett. **81** (1998) 2124.
 - [27] A. Ino, C. Kim, T. Mizokawa, Z.-X. Shen, A. Fujimori, M. Takabe, K. Tamasaku, H. Eisaki and S. Uchida: J. Phys. Soc. Jpn. **68** (1999) 1496.
 - [28] A. Ino, C. Kim, M. Nakamura, T. Mizokawa, Z.-X. Shen, A. Fujimori, M. Kakeshita, H. Eisaki and S. Uchida: cond-mat/9902048.
 - [29] See for example, T. Timusk and B. Statt: Rep. Prog. Phys. **62** (1999) 61.
 - [30] S. Uchida, T. Ido, H. Takagi, T. Arima, Y. Tokura and S. Tajima: Phys. Rev. B **43** (1991) 7942.
 - [31] T. Ido, K. Magoshi, H. Eisaki and S. Uchida: Phys. Rev. B **44** (1991) 12094.
 - [32] K. Machida and M. Ichioka: J. Phys. Soc. Jpn. **68** (1999) 2168.
 - [33] T. Tanamoto, H. Kohno and H. Fukuyama: J. Phys. Soc. Jpn. **62** (1993) 717, 1455; **63** (1994) 2739.
 - [34] L.F. Mattheiss: Phys. Rev. Lett. **58** (1987) 1028.
 - [35] J.-H. Xu, T.J. Watson-Yang, J. Yu and A.J. Freeman: Phys. Lett. A **120** (1987) 489.
 - [36] T. Tohyama, S. Nagai, Y. Shibata and S. Maekawa: Phys. Rev. Lett. **82** (1999) 4910.
 - [37] K. Kuroki, R. Arita and H. Aoki: Phys. Rev. B **60** (1999) 9850.
 - [38] G. Seibold, C. Castellani, C. Di Castro and M. Grilli: Phys. Rev. B **58** (1998) 13506.
 - [39] See for example, W.A. Harrison: *SOLID STATE THEORY* (Dover Publications, New York, 1980), Chap. III.
 - [40] R. Kubo: J. Phys. Soc. Jpn. **12** (1957) 570.
 - [41] D.A. Greenwood: Proc. Phys. Soc. (London) A **71** (1958) 585.